NUMERICAL INVESTIGATION OF SPARK-IGNITION IN A LAMINAR METHANE-AIR COUNTERFLOW

E. Richardson* and E. Mastorakos
***e-mail: esr24@cam.ac.uk**
Cambridge University Engineering Department,
Trumpington Street, Cambridge CB2 1PZ, UK

Abstract

Simulations of forced ignition in a non-premixed laminar counterflow are used to study the effect of the strain rate on ignition success. A one dimensional calculation is performed, using detailed methane chemical kinetics, and treating the ignition event as an instantaneous heat release. Ignition success is seen to depend on the mixture composition and spark location, resulting in lean and rich ignitability limits for a given spark that can be different from the nominal flammability limits. Ignition is also prohibited by excessive strain rates, in some cases at levels well below the extinction value. The structure of the evolving ignition region is examined in terms of its temperature, heat release rates and its composition. In the case of successful ignition, the high temperature reached due to the spark energy deposition causes local auto-ignition. Subsequently, intense burning rapidly consumes the reactants in the remaining region of flammable methane-air mixture. As this intense burning subsides a partially premixed and then a non-premixed diffusion flame are seen to survive.

Introduction

An improved understanding of mixture ignitability and the modeling of ignition events is needed for the satisfactory treatment of forced ignition in flows with wide variations in fuel concentration. Gas turbine combustors and atmospheric releases of flammable material provide important examples of such flows. Auto-ignition of non-premixed flow and the forced ignition of premixed flow are frequently studied, however there are aspects of the forced ignition of non-premixed fluid which require further fundamental investigation. Birch et al. [1] demonstrated the randomness spark ignition in a turbulent non-premixed jet flames. Alvani and Fairweather [2] proposed a largely successful model for the ignition probability of inhomogeneous mixtures in the terms of the probability of finding flammable mixture at the spark location. Ahmed and Mastorakos' measurements [3] of spark ignition in a turbulent jet show a number of fluid dynamic influences on the early kernel development in addition to the compositional effects. Simple chemistry DNS [4] shows the development of a tribrachial structure in a turbulent non-premixed flame kernel. Rashkovsky [5] used the laminar non-premixed counterflow as a paradigm for the flow processes relevant to the ignition of a turbulent inhomogeneous fuel-air mixture, and was able to demonstrate that fluid dynamics, as characterized by the chemical Damköhler number, have a rôle in determining the success of ignition.

The laminar counterflow configuration provides a well defined flow field in which to examine the effect of strain on flame structure, consequently it has provided significant insight to the study of turbulent non-premixed combustion [6]. The non-premixed configuration involving opposed jets of fuel and oxidizer has been used to investigate transient auto-ignition processes both numerically [7] and experimentally [8]. The configuration is also convenient for studies of some aspects of forced ignition processes. Forced ignition is distinguished from auto-ignition by the presence of a localized transient heat source. The heat source or *igniter* can take a variety of

forms, including heated surfaces, electrical sparks and laser pulses. Even igniters of the same type can have very different characteristics in terms of the spatial and temporal evolution of the energy input. Laser Induced Spark Ignition (LISI) delivers a measurable quantity of energy to the fluid at the focus of the laser over a relatively short period of time, 5-500ns [9]. The LISI process lends itself to a simple numerical representation as an instantaneous heat release, and the absence of a solid igniter in the interesting region of the flow is also an advantage.

A simulation of ignition in a laminar methane-air counterflow mixing layer, using LISI, has been devised in order to display the variety of ignition behaviour possible for a range of strain rates. Details of the flow and ignition formulation are given in the following section. The resulting ignitability limits are then discussed, and the transient flame structures are examined in order to discover the mechanisms which give rise to successful and failed ignition. The flame structures are presented in terms of mixture fraction, and neglecting topographical effects such as flame curvature, similar flame structures may be expected during the ignition of certain turbulent flows, for example a globally homogeneous turbulent flow with fuel-air segregation experiencing equivalent strain conditions.

Formulation

Flame Equations

The computational configuration is a non-premixed counterflow arrangement with planar geometry. RUN1DL is used to solve a low Mach number formulation of the flame equations in terms of a distance variable [10], including detailed molecular transport. Variable molecular properties and the GRI-Mech 3.0 detailed chemical scheme are employed for reactions between methane and air [11]. The 53 species GRI-Mech 3.0 which has been optimized for combustion of natural gas using data in the range 1000-2500 K, also shows realistic extinction behaviour. The solution is evaluated by integrating the system on an adaptive grid with a modified Newton method [10], ensuring grid independence of the solution. The fuel and air inlets are at y=-6 mm and y=6 mm respectively, and the boundary temperature and pressures are 293 K and 100 kPa. The stagnation point is fixed at y=0 and the inlet velocities are determined according to a specified strain value a_∞ [10]. The values of mixture fraction used to report data from the counter flow calculations are calculated using the nitrogen atom conservation.

Forced Ignition

The simulated LISI spark is considered to cause instantaneous heating of a volume with thickness Δy_{spark} =0.25mm, with a smooth temperature profile peaking at 4000K centred at y_{spark}. The initial condition used for calculations in this investigation is a converged inert flow with the spark's temperature profile subsequently imposed. The low Mach number formulation described above does not capture the pressure waves that result from the sudden temperature change, nor is the chemical mechanism valid at such a high temperature. The very early evolution of the chemical composition and of the velocity field should hence not be given undue credence. Despite the doubt this casts over the early transport of the spark energy, the total spark energy is conserved. Dissipative processes cause a rapid decrease of the peak temperature and the subsequent predictions of the chemical and thermal evolution are better founded.

We will be comparing the mixture fractions that ignite with the nominal static flammability limits of methane, which give ξ_{lean}=0.0284 and ξ_{rich}=0.089 [12].

Table 1. Details of Spark events A-C.

	a_∞ (s^{-1})	y_{spark} (mm)
Spark A	190.0	0.555
Spark B	190.0	0.689
Spark C	190.0	0.823

Results and Discussion

Ignition limits

Figure 1 shows the evolution of the temperature profile during a successful spark ignition, (Spark B). a_∞ =190.0 s^{-1} corresponds to 40% of the flame's extinction strain rate $a_{\infty,ext}$, found to equal 475.0 s^{-1} for the given boundary conditions. The equivalence ratio at the centre of the spark is lean. The peak temperature has decreased to 3848K within 2.0×10^{-7} s due to dissipation of the spark energy and an initial predominance of endothermic reactions. As the heat release increases the peak temperature briefly rises to 3868K at 1.0×10^{-6} s. Heat from the flame diffuses through the mixing layer, while the spark energy is dissipated, and a steady diffusion flame has been established by 1.0×10^{-2} s.

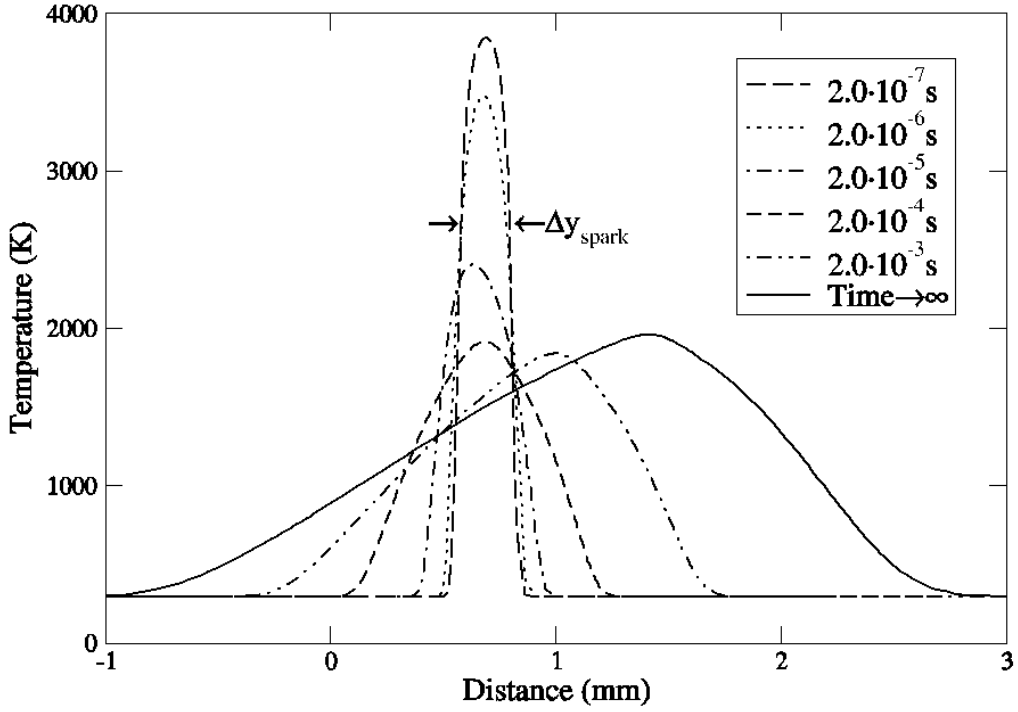

Figure 1. Transient temperature profiles in physical space during a successful ignition event, (Spark B).

Figure 2 shows the mixture fraction profile within the mixing layer in the unreacting flow before ignition and once the diffusion flame has stabilized. The changes in density as the flame is established cause significant expansion of the mixing layer. The shift in mixture fraction

contours can confuse analysis of the transient flame structure if viewed only in the spatial coordinate, and hence analysis is presented in terms of the mixture fraction.

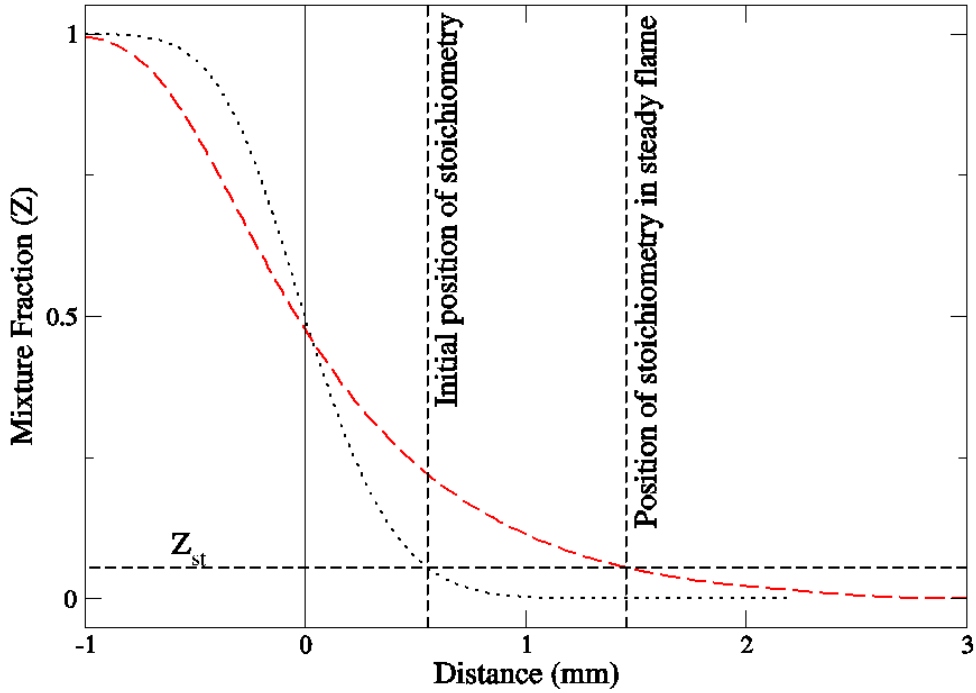

Figure 2. Mixture faction plotted in physical space for the case $a_\infty/a_{\infty,ext}$=0.4 showing the profile for inert mixing (dotted), and in the converged burning solution (dashed). The positions of the stagnation point and of stoichiometry in the inert and burning flow are also marked.

The locus of the mixing layer ignitability limits are shown in Figure 3 for a range of $a_\infty/a_{\infty,ext}$. Sparks centred within the closed locus result in successful ignition while sparks outside this region fail to cause ignition. The position coordinate has been transformed using the factor $(a_\infty/a_{\infty,ext})^{1/2}$ which is proportional to the physical width of the inert mixing layer [13]. Thus contours of mixture fraction are seen as vertical lines. The loci of stoichiometry and of the premixed flame static flammability limits [12] are also shown for comparison. The locations of sparks A-C are also plotted. Spark A is outside the lean ignitability limit and spark C is outside the rich ignitability limit, however spark B is in the ignitable region and leads to successful ignition.

The ignitable region in Figure 3 is fully enclosed by rich and lean ignitability limits which are wider than the static flammability limits. An important feature of Figure 3 is that ignition may be precluded above a critical value of strain rate, which doesn't change too much with spark location and which is lower than the extinction value.

The ignitability limits and the static flammability limits are expected to converge at the limit of zero strain, although this is not guaranteed since experimental and numerical results are being compared. It should be noted that the spark has a finite width of 0.25mm, which scales down to $\Delta y(a_\infty/a_{\infty,ext})^{1/2}$=0.0791 mm and 0.177 mm at $a_\infty/a_{\infty,ext}$=0.1 and 0.5 respectively. The spark's width is comparable to the width of the static flammability region, hence a large proportion of spark B resides inside the nominally flammable region. The locus of ignitability is plotted according to the position of a spark's centre. The lean ignitability limit is seen to lie some way

outside the lean static flammability limit, however an edge of the spark is always very close to the static limit and at $a_\infty/a_{\infty,ext}$ =0.1 one edge of the spark lies inside the static flammable limit.

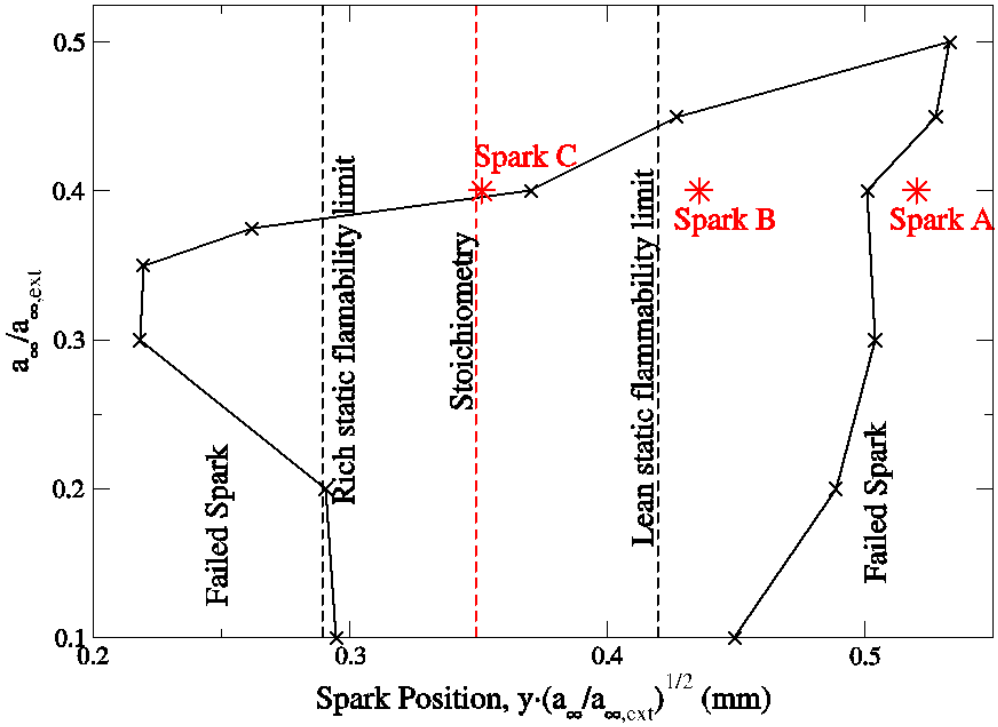

Figure 3. The locus of the mixing layer ignitability limits are shown for a range of $a_\infty/a_{\infty,ext}$. Vertical lines indicate the loci of stoichiometry and of the static flammability limits. The position of Sparks A-C are marked with stars.

Ignition evolution

Figure 4 shows the transient temperature profiles for sparks A,B and C in mixture fraction space. Spark A is located at a sufficiently lean mixture fraction that by the time appreciable spark energy arrives in the flammable region, the temperature has dropped too low for successful ignition. Spark B is successful. Spark C fails to ignite the flow despite sparking the entire flammable region. While spark C seems more promising than the leaner spark B, it should be noted that the scalar dissipation rate gets higher closer to the stagnation point where Z~0.5 and this apparently leads to the quenching of spark C.

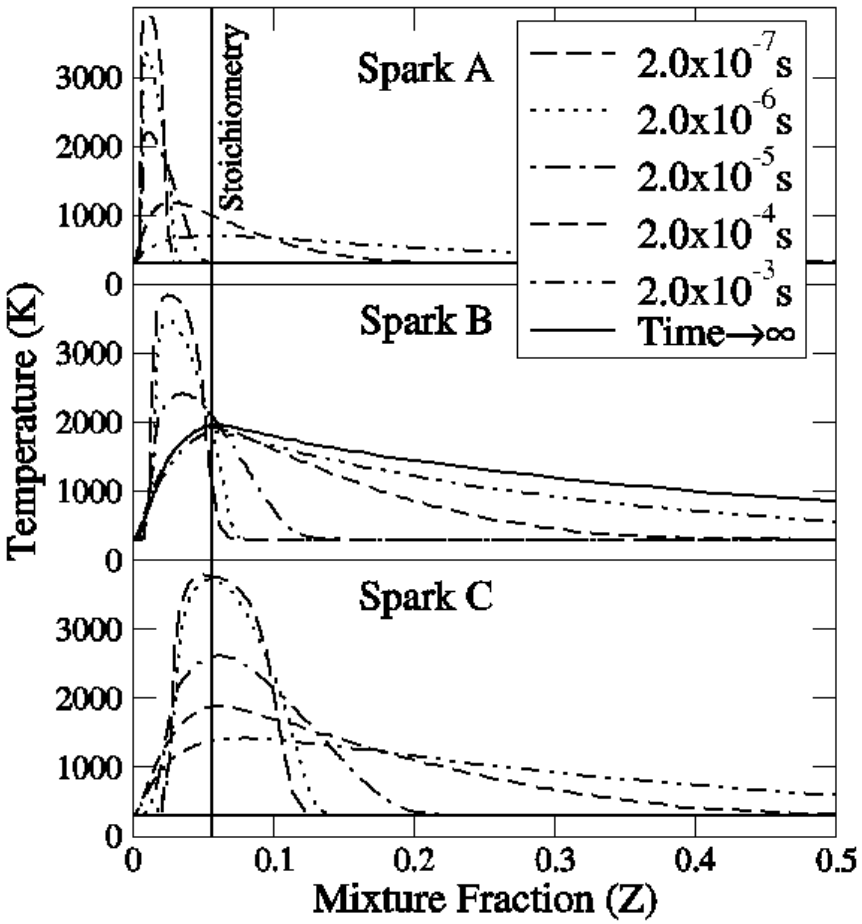

Figure 4. Transient temperature profiles in mixture fraction space for sparks A, B and C.

In case A, the consumption of oxygen and methane is very limited, (Figure 5). In case B the reactants are initially consumed in the region of the spark and subsequently the premixed reactants from outside the spark region are consumed until a pure diffusion flame is achieved. The flame structure during this partially premixed phase is not clear from Figure 5, however it involves a flame front propagating across the flammable region away from the spark. The flame front is thought to fade as it reaches the edge of the flammable mixture and subsequent burn out of the oxygen contained in the rich mixture takes place in a single partially premixed diffusion flame close to stoichiometry, eventually becoming a non-premixed diffusion flame as the flow stabilizes. In case C, a large proportion of the reactants is consumed within the spark region, however there is greater fuel leakage than in case B. Consumption of the surrounding cold premixed reactants proceeds, but the flame is quenched before the stable diffusion flame condition is achieved.

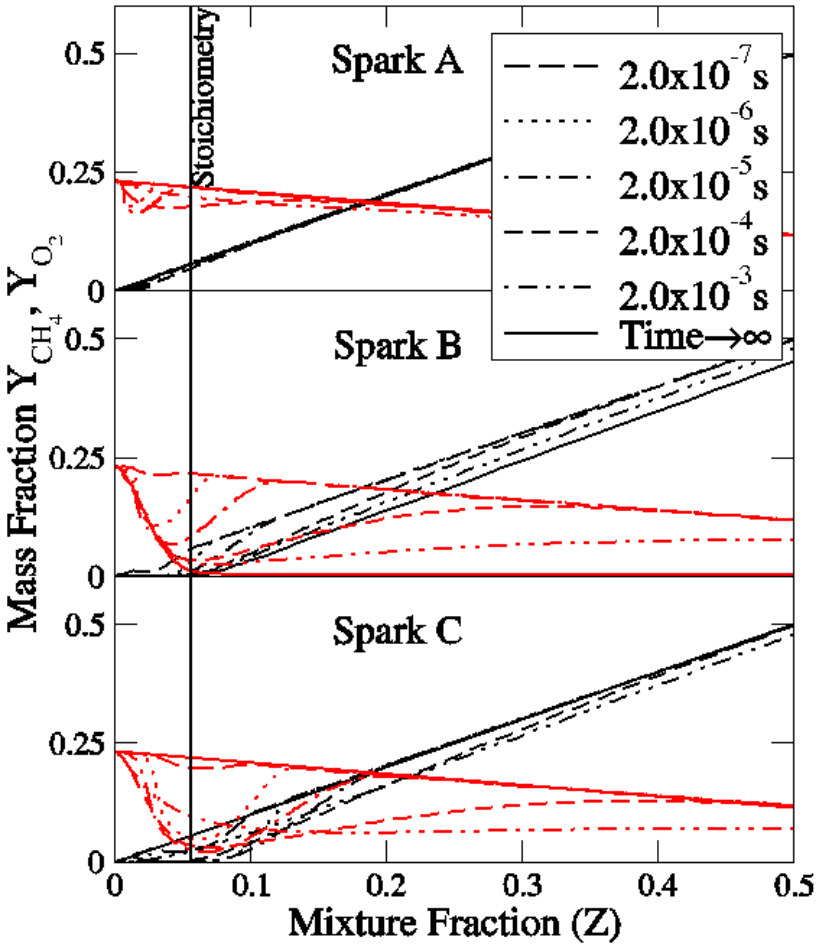

Figure 5. Transient mass fraction profiles in mixture fraction space for the two primary reactants, methane and Oxygen, for sparks A,B and C.

The initial, strongly endothermic heat release values seen in Figure 6 are very short lived ($t<10^{-6}$ s), and are replaced by an exothermic heat release profile with peaks close to both the rich and lean edges of the spark. While the small physical size of the inflamed region may make it inappropriate to discuss individual flame fronts, the large heat release rates at the edges of the burning regions, rather than close to stoichiometry early on, indicate that premixed type reaction zones dominate for around $2.0\text{x}10^{-4}$ s. For successful ignition it is then necessary to stabilize a diffusion flame, as is seen in the case of spark A. The flame structure involving rich and lean fronts and an inner diffusion flame may be described as tribranchial. The flame evolution observed here is comparable to that observed in the DNS studies of the forced ignition [4] and auto-ignition [14] of turbulent non-premixed flows.

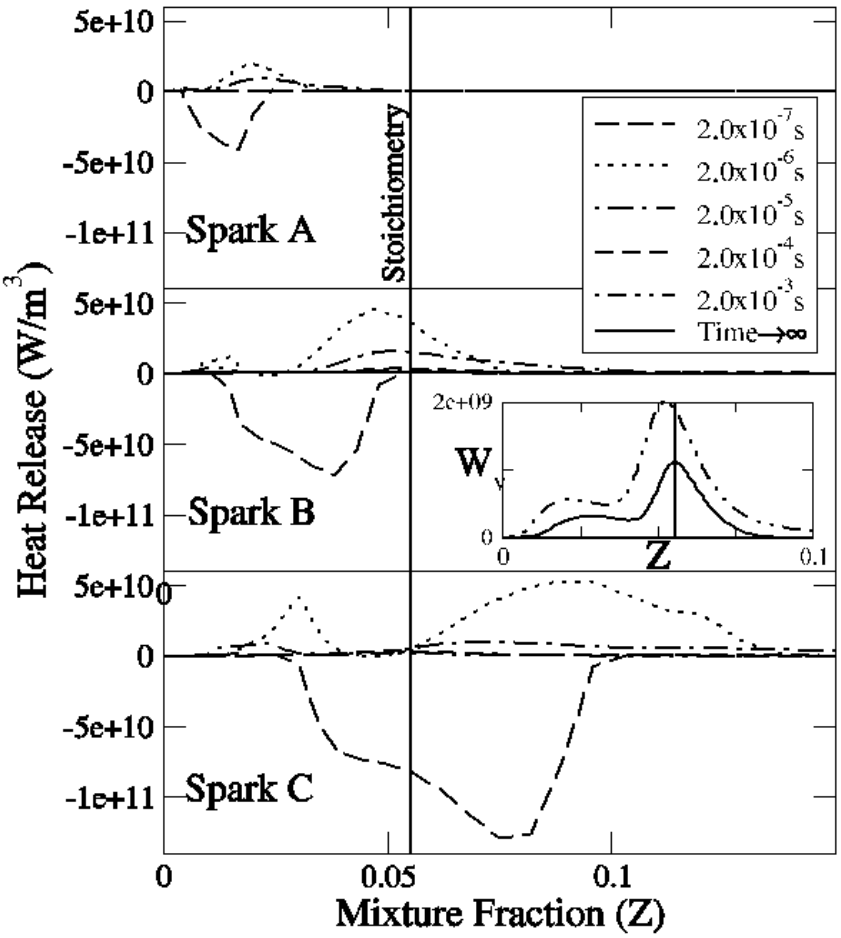

Figure 6. Transient heat release profiles in mixture fraction space for sparks A,B and C. The inset graph is an enlargement showing the stabilized heat release profile for case B.

The evolution of the OH radical's concentration is reported in Figure 7. In agreement with experimental observations [15], the predicted transient OH concentration peaks at around an order of magnitude higher than in the steady diffusion flame, and then it decays while the temperature falls. The shape of the OH profile reflects that of the temperature rather than the heat release.

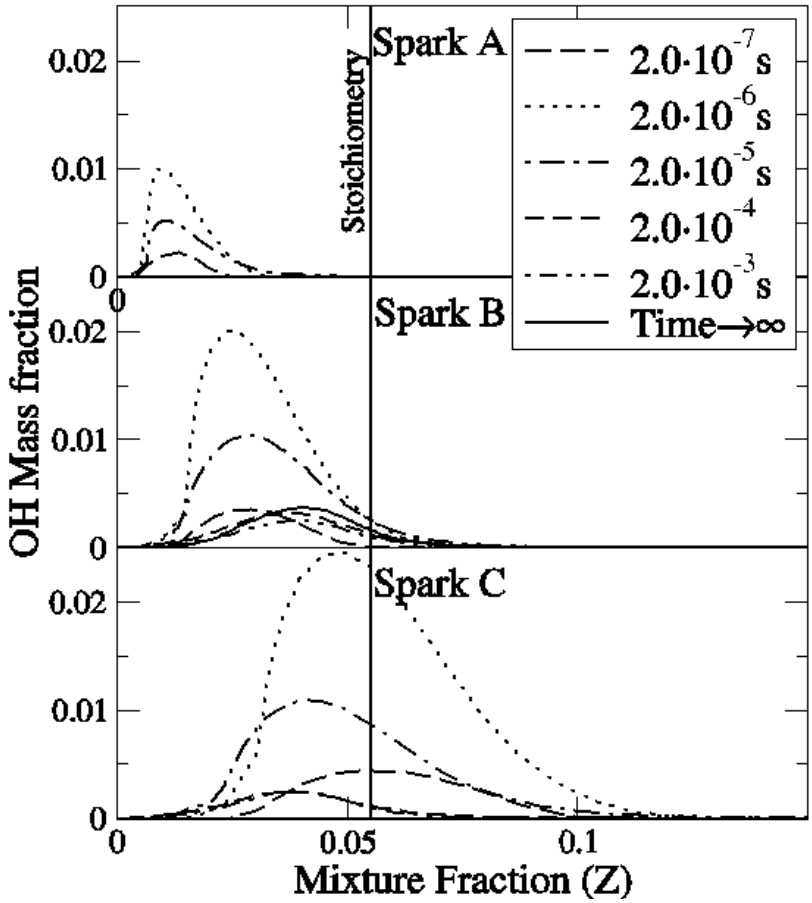

Figure 7. Transient OH mass fraction profiles in mixture fraction space for sparks A, B and C.

Conclusions

A non-premixed laminar counterflow with a particular set of boundary conditions has a critical strain rate, which is dependent on the igniter, above which forced ignition is impossible. This value is less than the extinction strain rate at which a steady flame becomes impossible.

Analysis of the transient flame structure during successful forced ignition show that once reactants have been consumed in the ignition region, there are some indications that premixed flame fronts may exist at the edges of the ignition region. As the spark energy is dissipated, the premixed fronts become less distinct and are dominated by a partially premixed diffusion flame which burns the remaining premixed reactants and finally stabilizes as a non-premixed diffusion flame.

Failure to ignite in particular regions of a laminar non-premixed flow is due to a combination of excessive dissipation and the local mixture flammability. Regions of very low scalar dissipation rate can have insufficient fuel to ignite, while otherwise flammable regions can fail to ignite due to the local dissipation rate being too high.

References

[1] Birch, D.R., Lefebvre, A.H., *Combust. Flame* 35, 155-168, (1979)
[2] Alvani,R.E. and Fairweather,M.,*Trans. of Ichem E*, 80,917-923, (2002).
[3] Ahmed, S.F. and Mastorakos, E., submitted to *Combust. Flame, (2005)*.
[4] Chakraborty, N. and Mastorakos, E., submitted to *Fourth Mediterranean Combustion Symposium*, Lisbon, October 2005.
[5] Rashkovsky, S.A., *First Mediterranean Combustion Symposium*, Antalya, Turkey, June 1999, p.1403-1411.
[6] Peters, N., *Turbulent Combustion*. Cambridge, 2000.
[7] Gopalakrishnan, V. and Abraham, J., *Combust. Flame,* 136, 557-566, (2004).
[8] Fotache, C.G., Kreutz T.G., and Law, C.K., *Combust. Flame*, 108, 442, (1997).
[9] Phuoc, T.X., White, C.M., and McNeill, D.H., *Optics and Lasers in Engineering*, 38, 217-232, (2002).
[10] COSILAB. The Combustion Simulation Laboratory, Version 1.1. www.SoftPredict.com, Rotexo GmbH & Co. KG, Haan (Germany), 2005.
[11] Gardiner, B., Yang, H., Quin, Z., Smith, G., Crosley, D., Golden, M., Bowman, T., Hanson, R., Davidson, D., Frenklach, M., Moriarty, N., and Eiteener, B. http://me.berkeley.edu/gri_mech.
[12] US Environmental Health and Safety. Material safety data sheet. Technical Report M2015, Mallickrodt Baker inc., (2004)
[13] Pitsch, H. and Peters, N., *Combustion and Flame*, 114:26-40, (1998).
[14] Mastorakos, E.,Baritaud, T.A., and Poinsot, T.J., *Combust. Flame*, 109, 198-223, (1997).
[15] Thiele, M., Warnatz, J., Dreizler, A., Lindenmaier, S., Schiebl, R., Maas, U., Grant, A., and Ewart, P., *Combust. Flame*, 128, 74-87, (2002).